applied sciences

MDPI

Article

Strategy for Visual Measurement of Power Quality Based on Higher-Order Statistics and Exploratory Big Data Analysis

Juan-José González-de-la-Rosa *, Olivia Florencias-Oliveros and Paula Remigio-Carmona

Research Group PAIDI-TIC-168, Department of Automation Engineering, Electronics, Architecture and Computers Networks, University of Cadiz, 11202 Algeciras, Cadiz, Spain; olivia.florencias@uca.es (O.F.-O.); paula.remigio@uca.es (P.R.-C.)

* Correspondence: juanjose.delarosa@uca.es

Featured Application: The proposed visualization strategy can be applied in power quality monitoring systems to detect and characterize non-Gaussian disturbances caused by non-linear loads. It is especially useful for engineers and analysts working with large-scale energy data, supporting more efficient energy data management and cost optimization in industrial and smart grid environments.

Abstract: This article proposes a strategy for the visual characterization of power quality in big data analysis contexts, culminating in the development of a visualization tool based on higher-order statistics, which exhibits an efficiency between 83.33% and 100% in detecting 50 Hz synthetic and real-life simple and hybrid events, showing its significant potential for real-world applications marked by non-linear loads and non-Gaussian behaviors and surpassing the detection of traditional tools such as boxplot by up to 50%. Efficient energy management is closely accompanied by an optimum energy data management (EDM). It implies the acquisition, analysis, and interpretation of data to make decisions regarding the best energy usage with subsequent cost reductions. Through a study of indicators, including higher-order statistics, crest factor, SNR and THD, the article establishes nominal values and behavioral patterns, expanding the previous knowledge of these parameters. The indicators are presented as vertices in a radar-type charting tool, providing a multidimensional spatial visualization from individual indices that allows the behavioral pattern associated with each type of disturbance to be characterized combined with a decision tree. In addition, boxplots reflecting data processing are included, which facilitates the comparison and discussion of both visualization instruments: radar chart and boxplot.

Keywords: higher-order statistics; observational data analysis; power quality; signal processing; visualization tool

Academic Editors: Santiago Bogarra and Juan Antonio Ortega-Redondo

Received: 30 April 2025
Revised: 30 May 2025
Accepted: 6 June 2025
Published: 7 June 2025

Citation: González-de-la-Rosa, J.-J.; Florencias-Oliveros, O.; Remigio-Carmona, P. Strategy for Visual Measurement of Power Quality Based on Higher-Order Statistics and Exploratory Big Data Analysis. *Appl. Sci.* **2025**, *15*, 6422. https://doi.org/10.3390/app15126422

1. Introduction

The increasing prevalence of non-linear loads in the electrical grid has led to an unprecedented demand for efficient power quality (PQ) management. PQ, crucial for maintaining the stability of electrical supply, directly impacts the performance of sensitive electronic equipment. Voltage fluctuations, hybrid disturbances, and other disturbances can significantly affect both consumer comfort and productivity [1]. Although current standards, e.g., EN 50160 [2], offer substantial utility in network maintenance, they may nevertheless not cover the broad spectrum of electrical disturbances caused by modern non-linear loads, prompting the need for complementary detection methods. Similar challenges have been observed in other signal processing domains, where the limitations of

single-indicator approaches have led to the adoption of multi-indicator or source separation strategies [3].

This research focuses on developing a data visualization system based on exploratory data analysis (EDA) through a radar chart, aiming to provide tools to assess power grid health. Over the past quarter century, various methods for detecting PQ disturbances have been forged, which are all aimed at improving power quality in electrical systems [4]. Among them, artificial intelligence (AI) techniques—such as machine learning or fuzzy logic—stand out for their efficiency in classifying power quality events [5–7]. To enhance usability, this research incorporates a rule-based decision tree, allowing users, such as plant operators or non-experts, to engage with the diagnostic process without requiring specialized knowledge. The method combines visual results with detailed information about disturbances. Additionally, the low computational demand of this approach, compared to other methodologies [8], facilitates its integration into software or web-based applications.

The following sections detail the development and validation of this visual tool and decision tree based on both traditional and non-traditional indicators, including higher-order statistics (HOS). The system's performance will be validated with real and synthetic signals, aiming to combine simple result interpretation with low computational cost. Section 2 reviews related works in PQ monitoring. Section 3 describes the methodology followed for developing the system and signal processing. Section 4 details the system's testing process, and Sections 5 and 6 present discussions and conclusions, respectively.

2. Background Research

A thorough literature on power quality monitoring and electrical network disturbances reveals a growing adoption of HOS in recent years. However, limited attention is given to fifth- and sixth-order statistics. While these indicators are explored in [9–11], they lack nominal value characterization for power signal analysis and their boundaries under events. For instance, ref. [10] focus on HOS for signal characterization, encompassing both normal operation and a series of disturbances, both simple and complex, underscoring the effectiveness of HOS in power quality monitoring but without defining indicators' nominal values. In contrast, ref. [11] estimates nominal values on even-order HOS, including kurtosis at -1.5 and the sixth-order statistic at -6.2 for a 50 Hz signal. Similarly, ref. [9] suggests nominal values of zero, -1.5, zero and 2.48 for the third-, fourth-, fifth-, and sixth-order statistics, respectively. However, these values differ from those in [12,13], where kurtosis is reported around 1.5. Furthermore, no consensus exists regarding the nominal value of the sixth-order moment. These references highlight one of the main disadvantages of using HOS: the difficulty in interpreting results [14]. Nevertheless, integrating additional indicators into the radar chart helps mitigate this issue.

In recent studies, researchers are increasingly moving away from using a single indicator for PQ assessment, opting instead for a combination of tools. For instance, [9,11] use various statistics, while [15] mentions the use of multiple indicators, including the crest factor, total harmonic distortion, and K-factor, for transient disturbance detection. Feature extraction from both time and frequency domains is discussed in [16], while [17] combines HOS and RMS for hybrid event detection. Similarly, ref. [18] uses multiple indicators like skewness, kurtosis, entropy, crest factor, and form factor to detect simple and complex events, a methodology also employed by Shen et al. [19] and Thirumala et al. [20], who classify PQ events using six key features.

Unique visualization methods have also emerged to represent electrical disturbances. For example, ref. [12] introduces 2D diagrams showing signal state evolution during disturbances, leading to the development of the HOS Fingerprint tool for steady-state analysis [21]. In [22], a novel approach is proposed to detect abnormal operations, though

these methods can be difficult for average users to interpret. Thus, the focus has shifted toward more accessible visualization tools, such as those outlined in [23,24], which use color-based indicators and localized event depiction. However, these tools often rely on standards that may not fully capture the complex behavior of modern electrical loads.

3. Material and Methods

Following the review presented in Section 2, a curated selection of indicators has been chosen to underpin the development of a power quality visualization tool and a rule-based decision tree. All these elements are described below.

3.1. Databases

Both for calibration of the visual tool and for the study of the indicators and the decision tree, two different databases are used:

1. Synthetic Power Quality Disturbances—Database #1. This database comprises 1415 synthetic signals operating at 50 Hz, featuring flicker, harmonics, impulsive and oscillatory transients, interruption, notch, spike, sag, swell, harmonics with sag, and harmonics with swell. Signals with different degrees of noise contamination have been also considered. These signals have a duration of 0.2 s and sampling frequency of 3.2 kHz. The authors elaborate in MATLAB, version 9.10.0.1684407, through the tool proposed by Machlev et al. [25].
2. Real-life Power Quality Events—Database #2. Two datasets are included within this database. The first one, real-life power quality sags [26], encompasses 30 50 Hz signals, which are marked by sag events. The second dataset, real-life power quality transients [27], is composed of 42 50 Hz signals with the presence of impulsive transient. Signals in both datasets have durations of 1 s and sampling frequency of 20 kHz.

Throughout the next sections, signals with synthetic origin coming from Database #1 have been named S-[Event], while real signals coming from Database #2 use the R-[Event] nomenclature.

3.2. Indicators–Radar Chart Vertices

This section includes the features selected for the power quality visualization tool and the decision tree. These parameters have been previously studied and compared using the signals available in Database #1.

1. Skewness (Sk). The nominal value for skewness in 50 Hz signals is zero. Its deviation from this expected value is linked to the symmetry of the waveform. Generally, skewness is expressed by Equation (1). In Equations (1)–(4), x_j is a sample register measured from 1 to sample size, N, and σ corresponds to standard deviation.

$$Sk(x) = \frac{1}{N}\sum_{j=1}^{N}\left[\frac{x_j - \overline{x}}{\sigma}\right]^3 \quad (1)$$

2. Kurtosis (K). Based on our own tests with undistorted 50 Hz signals, we observed nominal kurtosis value of 1.5, which is used here as a reference. Kurtosis variations are linked to the sinusoidal shape of the waveform. K is given by

$$\mathrm{K}(x) = \frac{1}{N}\sum_{j=1}^{N}\left[\frac{x_j - \overline{x}}{\sigma}\right]^4 \quad (2)$$

3. Fifth-order statistic (FOS). Our research coincides with the only identified reference for the nominal value of the fifth-order statistic in 50 Hz, zero [9]. FOS is defined by

$$FOS(x) = \frac{1}{N}\sum_{j=1}^{N}\left[x_j - \overline{x}\right]^5 \quad (3)$$

4. Sixth-order statistic (SOS). Given the absence of a universally agreed upon nominal value for the sixth-order statistic, the authors have taken as reference the nominal value obtained after the analysis of Database #1, which yielded results of a nominal value of 0.3125 for this statistic. SOS is calculated using

$$SOS(x) = \frac{1}{N}\sum_{j=1}^{N}\left[x_j - \overline{x}\right]^6 \quad (4)$$

5. Crest factor (CF). Signals characterized by 50 Hz, distortion-free waveforms should manifest a crest factor of 1.4142. CF serves as an indicator of non-sinusoidal conditions, measuring how much the top of the sine wave is distorted, thus making it a valuable parameter for quantifying harmonic distortion. CF is determined by

$$CF = \frac{V_{peak}}{V_{rms}} \quad (5)$$

6. Signal-to-Noise Ratio (SNR) represents a commonly used metric within the realm of communication systems. The SNR serves to quantify the relationship between the desired signal and undesired noise within a signal, thereby indicating that a higher SNR corresponds to superior signal quality. This parameter has garnered attention in various research efforts [28,29]. Although there are no universally recognized standards for power quality monitoring, some authors establish a range between 30 and 70 dB for real signals [30,31]. SNR is expressed by Equation (6), where P_S is signal power and P_N is noise power.

$$SNR = 10 \cdot \log\left(\frac{P_s}{P_N}\right) \quad (6)$$

7. Total Harmonic Distortion (THD) measures the harmonic distortion present in a signal by comparing the sum of the powers of all harmonic components to the power of the fundamental frequency. The standard IEC 61000-4-7 [32] outlines that THD should be inferior to 8%. THD is given by Equation (7), where $V_{n\text{-}rms}$ is the RMS value of the nth harmonic component and $V_{fund\text{-}rms}$ is the RMS value of the fundamental component.

$$THD = \frac{\sqrt{\sum_{n=2}^{\infty} V_{n\text{-}rms}^2}}{V_{fund\text{-}rms}} \quad (7)$$

3.3. Visual Tool

To concisely bring together these indicators, a radar chart was selected, wherein each vertex corresponds to a specific indicator, which will show the evolution per cycle of the signal.

As part of the normalization process, indicators are meticulously normalized and biased to mitigate any potential issues arising from their diverse scales. As a result, an ideal sinusoidal signal will form a regular heptagon, as depicted in Figure 1a, establishing an ideal pattern. However, when the signal is under an event, this structured pattern

undergoes distortion, adapting to the fluctuations in the waveform, as exemplified in Figure 1b.

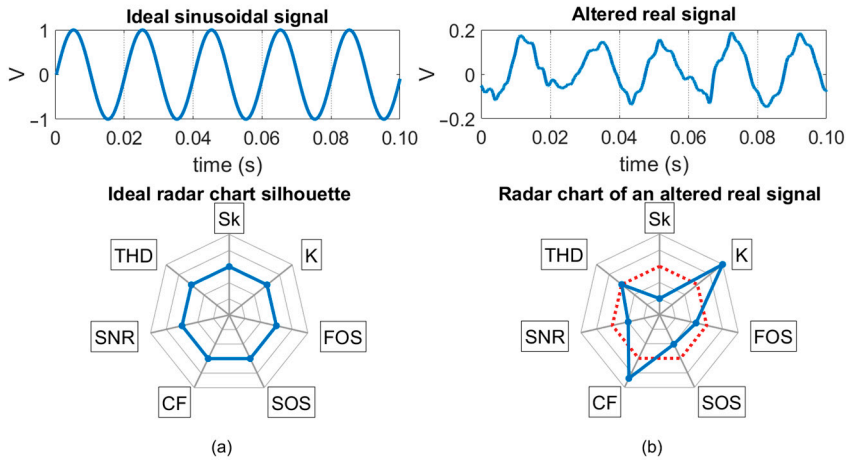

Figure 1. Radar chart from: (**a**) an ideal sinusoidal signal, (**b**) an altered signal. The ideal shape is highlighted in red for clarity.

A radar chart is generated per cycle, illustrating the progression of HOS and CF cycle by cycle, as well as a single SNR value per signal and a THD value per 10 cycles. In order to optimally cover the entire spectrum of PQ's phenomena analyzed, the axes corresponding to skewness, kurtosis, fifth-order statistics, crest factor and SNR follow a linear function, while SOS and THD are governed by a logarithmic function. This distinction is based on the distribution properties of each indicator: SOS and THD typically span a wide range of values with a strong skew toward the upper end, while their nominal values lie closer to the lower bound of their scale. A logarithmic scale enhances resolution in their most informative ranges. In contrast, the remaining indicators vary more symmetrically around their nominal values, for which a linear scale provides clearer visual interpretation. The axles' limits are specified in Table 1.

Table 1. Axles' limits.

Axis	Upper Limit	Lower Limit
Sk	0.31	−0.31
K	1.80	1.20
FOS	0.17	−0.17
SOS	10.63	0
CF	2.51	0.32
SNR	160	0
THD	22	0

Furthermore, the functions governing the visualization of each axis are based on conditions that allow for both the display of all event types and the maintenance of a regular heptagonal silhouette in the absence of disturbances. On the one hand, for all indicators, large outlier values are biased toward the limits of each axis, so the outliers are detected without impairing the visualization of other, less significant events. On the other hand, indicators like SNR, whose ideal value is 80 dB or higher, or THD, where harmonic presence is not considered below 8%, do not have a single optimal or nominal value. Therefore, to ensure an optimal radar display with a regular shape, SNR values greater than 80 dB are shown as 80 dB on the radar chart. Similarly, THD values below 8% will be represented as 8%.

To support the adequacy of these visualization decisions, a sensitivity analysis was conducted using synthetic signals. For selected events, multiple radar charts were simulated with different scaling functions, and the configuration that offered the best performance across the studied events was ultimately selected. Figure 2 illustrates two representative comparisons: in Figure 2a, a radar chart with axis ranges based on the maximum values observed in the dataset is compared to the optimized model under a notch event; in Figure 2b, a chart with more compressed axes is compared to the optimized model under Gaussian noise (40 dB). The results showed that excessively wide axis ranges can visually suppress distortions caused by events such as notch, rendering them indistinguishable. Conversely, overly narrow ranges tend to amplify irrelevant fluctuations due to noise, especially in real measurements, potentially leading to false detections. Moreover, they may obscure the evolution of indicators during an event.

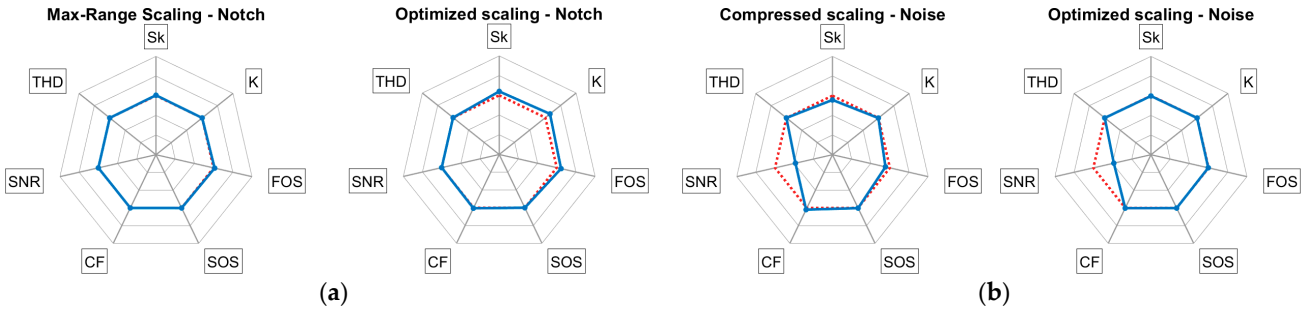

Figure 2. Comparison of different radar chart scaling approaches under (**a**) a notch event; (**b**) 40 dB Gaussian noise.

Additionally, boxplots are used to visualize the information extracted from each signal. The statistical method, shown in Figure 3, allows visually summarizing the distribution and variability of a data set, making it easy to identify extreme values and providing a quick overview of how the data are distributed. Therefore, this approach enables the examination and comparison of the distribution of values assumed by each indicator used in the proposed radar chart tool. Given the varying scales of these indicators, a normalization process becomes imperative. As a result, indicators are normalized to ensure their values fall within the range of -1 to 1, with the optimal indicator value remaining at zero, while the most unfavorable case is represented at either +1 or -1.

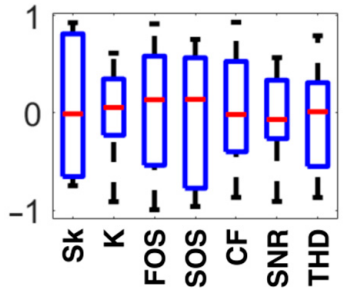

Figure 3. Boxplot's example of indicators based on a normal distribution. However, in real power quality analysis, maximum values of approximately ± 1 will occur in especially unfavorable cases but not uniformly across all indicators.

The determination of both ranges for the radar chart and boxplot has been empirically established following an in-depth analysis of Database #1 detailed previously.

3.4. Decision Tree

In addition to the radar chart, the authors have developed a decision tree that classifies the type of event based on the values measured by the indicators following the statements shown in Figure 4. The following specific terms are used in the decision tree (these terms are more fully explained in the Results section):

- Transitional values: values acquired by Sk, K, FOS and CF in signal transition cycles, different of nominal values (NV in Figure 4). These thresholds were empirically defined and depend on the location or site where the measurements are developed.
- Differentiating value: value acquired by SOS that allows differentiating sags from interruptions.

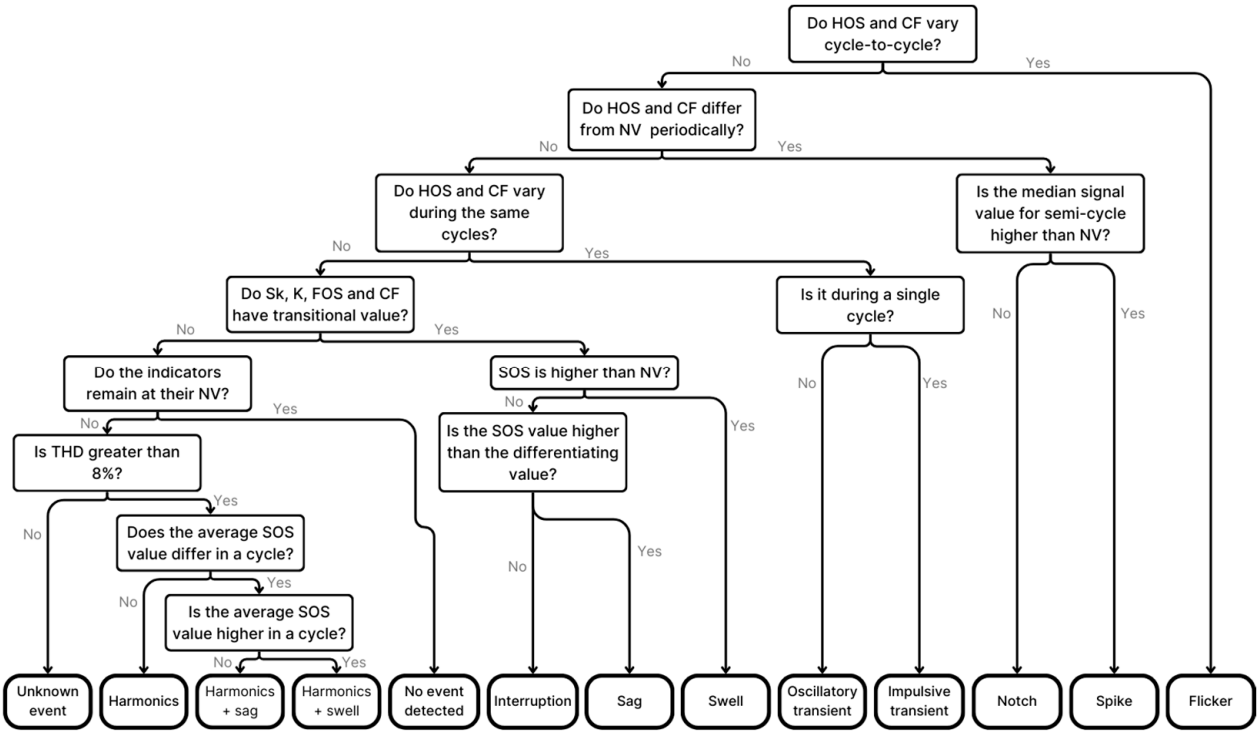

Figure 4. Decision tree scheme method for power quality event classification.

The methodology for developing the system is structured as follows in Figure 5:

1. Calibration with synthetic signals: initially, signals are extracted from Database #1. Maximum, minimum, and nominal values for each indicator are studied. These values have defined the limits for radar chart vertices and boxplot normalization.
2. Observation of indicators' behavior patterns under different events from Database #1: indicators' behavior is reflected per cycle in the radar chart, obtaining specific patterns for each type of event. This behavior is also applied for the development of decision tree statements.
3. Signal processing and comparative analysis: each signal is analyzed in three ways: (a) generating radar charts per cycle, illustrating the signal's evolution, (b) drawing a boxplot per signal that compiles all values per indicator, and (c) decision tree results per signal. These analyses are compared, and subsequently, the correspondence in behavior of the same event extracted from two different databases is also compared.
4. Determination of tool accuracy. Once all the signals available in both databases have been processed, the percentage of events satisfactorily located by each tool, radar chart with decision tree and boxplot, is obtained. The tool accuracy will be explained in Section 4.3.

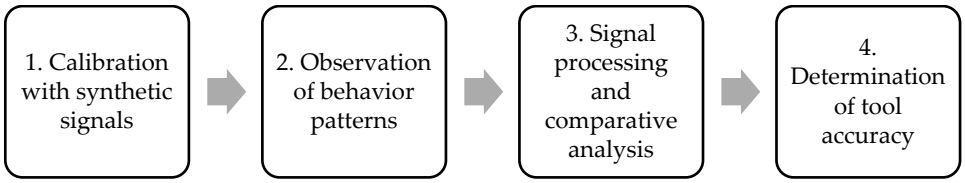

Figure 5. Process chart of the methodology followed for the development of radar charts.

4. Results

4.1. Behavior Patterns per Event

Hereinafter, different events related to synthetic signals and real signals are analyzed from the time domain. Depending on the type of event, the waveform undergoes a specific evolution. To define the type of evolution, three possible states are differentiated within a signal:

- The first state (state I) corresponds to the ideal scenario of a 50 Hz electrical signal. In the context of synthetic noise-free signals, this state represents an ideal condition. In real signals, this state is indicative of minimal disturbances that do not significantly impact the network's performance.
- State II in a signal represents an unstable phase under an event. This instability may encompass the entire event or just a part of it (in that case, state II is a transitional state between states I and III), as discussed below.
- State III also occurs when the signal is under an event. Unlike state II, state III implies stability of the waveform under the event.

Subsequently, Figures 6–15 show the list of events studied in Database #1. The signal states are distinguished, and an example of the pattern corresponding to each state per event is shown. The radar charts corresponding to state I have been omitted, since for these synthetic noise-free signals, the shape corresponds to the same behavior pattern shown in Figure 1a. Square marks have been added to each radar chart illustrating the maximum and minimum values that each indicator reach for the corresponding event and state. These values are also detailed in Tables 2–12.

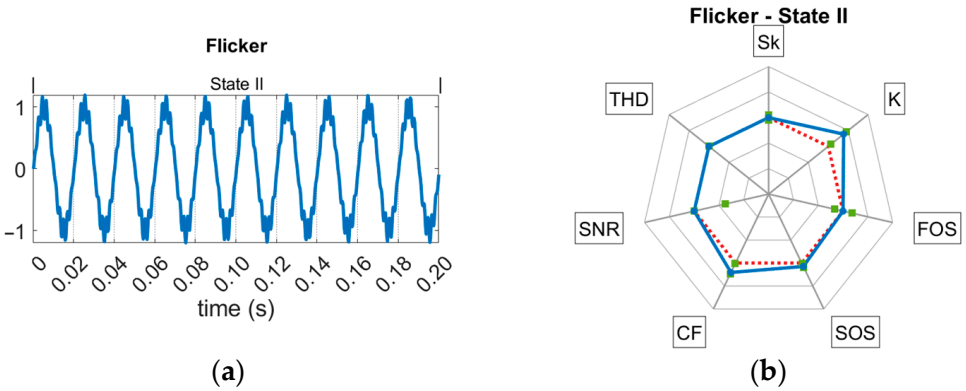

Figure 6. (**a**) Ficker signal; (**b**) state II behavior pattern for flickers. Blue line designates the current shape, the red line shows the ideal shape, and the green square marks illustrate maximum and minimum values.

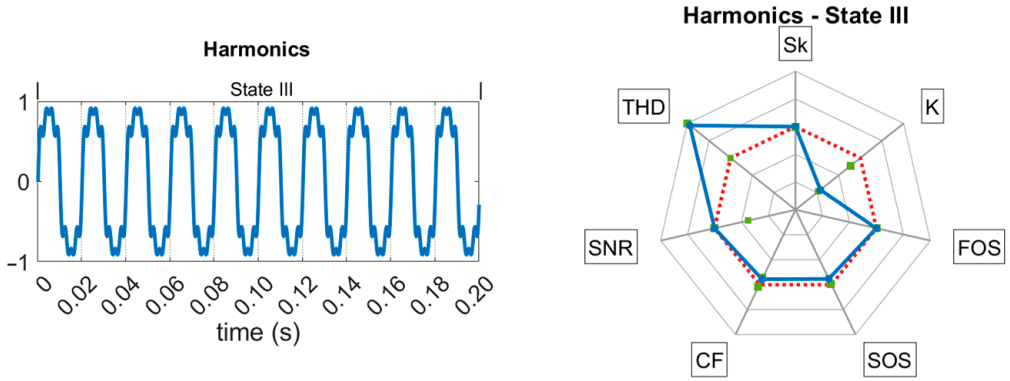

(**a**) (**b**)

Figure 7. (**a**) Harmonics signal; (**b**) state III behavior pattern for harmonics. Blue line designates the current shape, the red line shows the ideal shape, and the green square marks illustrate maximum and minimum values.

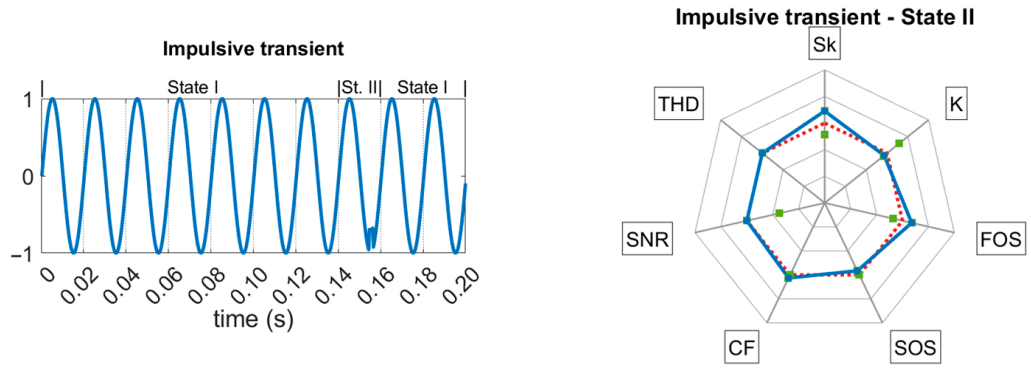

(**a**) (**b**)

Figure 8. (**a**) Impulsive transient signal; (**b**) state II behavior pattern for impulsive transients. Blue line designates the current shape, the red line shows the ideal shape, and the green square marks illustrate maximum and minimum values.

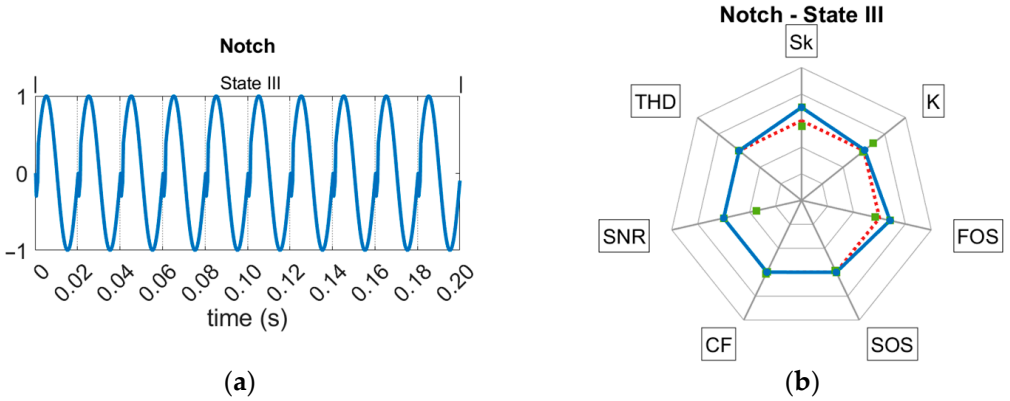

(**a**) (**b**)

Figure 9. (**a**) Notch signal; (**b**) state III behavior pattern for notches. Blue line designates the current shape, the red line shows the ideal shape, and the green square marks illustrate maximum and minimum values.

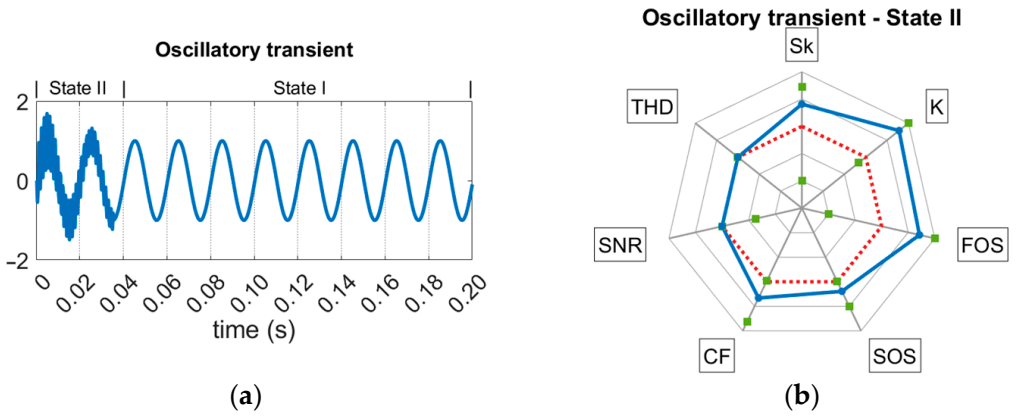

(**a**) (**b**)

Figure 10. (**a**) Oscillatory transient signal; (**b**) state II behavior pattern for oscillatory transients. Blue line designates the current shape, the red line shows the ideal shape, and the green square marks illustrate maximum and minimum values.

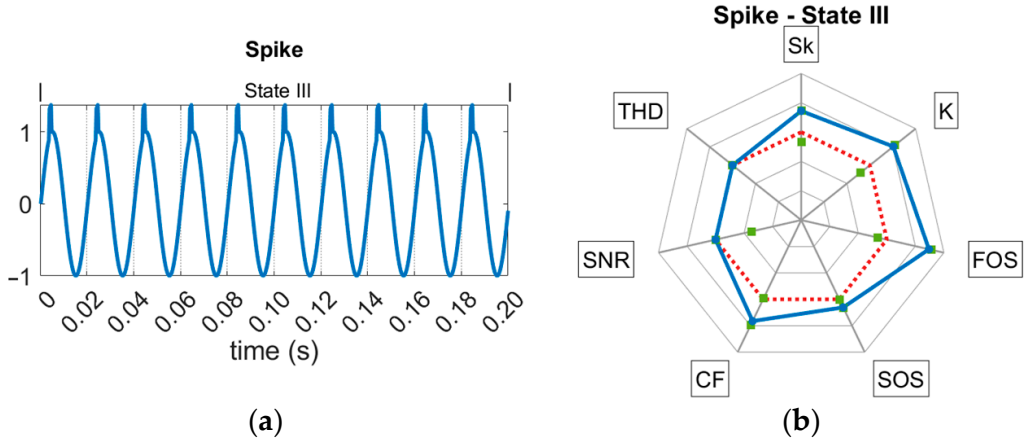

(**a**) (**b**)

Figure 11. (**a**) Spike signal; (**b**) state III behavior pattern for spikes. Blue line designates the current shape, the red line shows the ideal shape, and the green square marks illustrate maximum and minimum values.

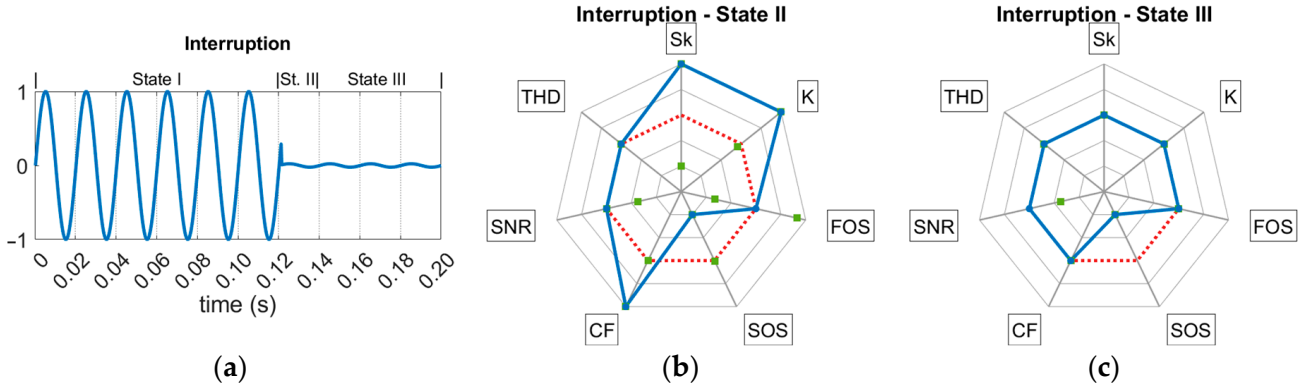

(**a**) (**b**) (**c**)

Figure 12. (**a**) Interruption signal; (**b**) state II behavior pattern for interruptions; (**c**) state III behavior pattern for interruptions. Blue line designates the current shape, the red line shows the ideal shape, and the green square marks illustrate maximum and minimum values.

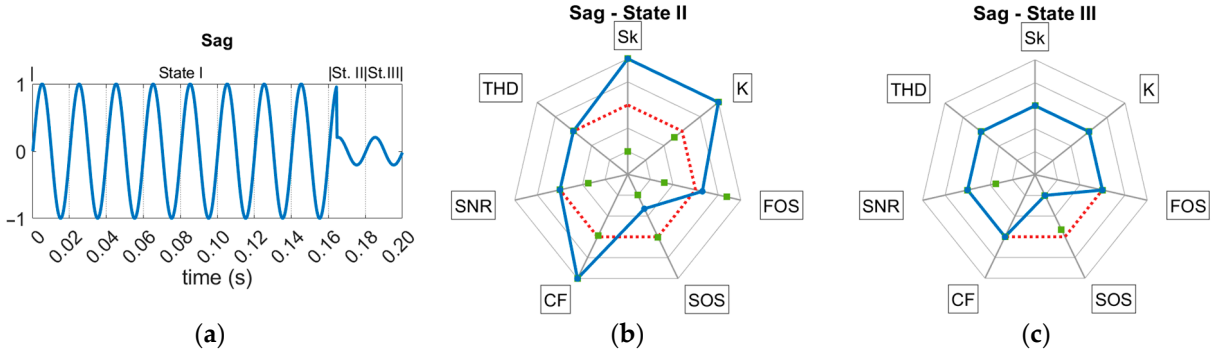

Figure 13. (**a**) Sag signal; (**b**) state II behavior pattern for sags; (**c**) state III behavior pattern for sags. Blue line designates the current shape, the red line shows the ideal shape, and the green square marks illustrate maximum and minimum values.

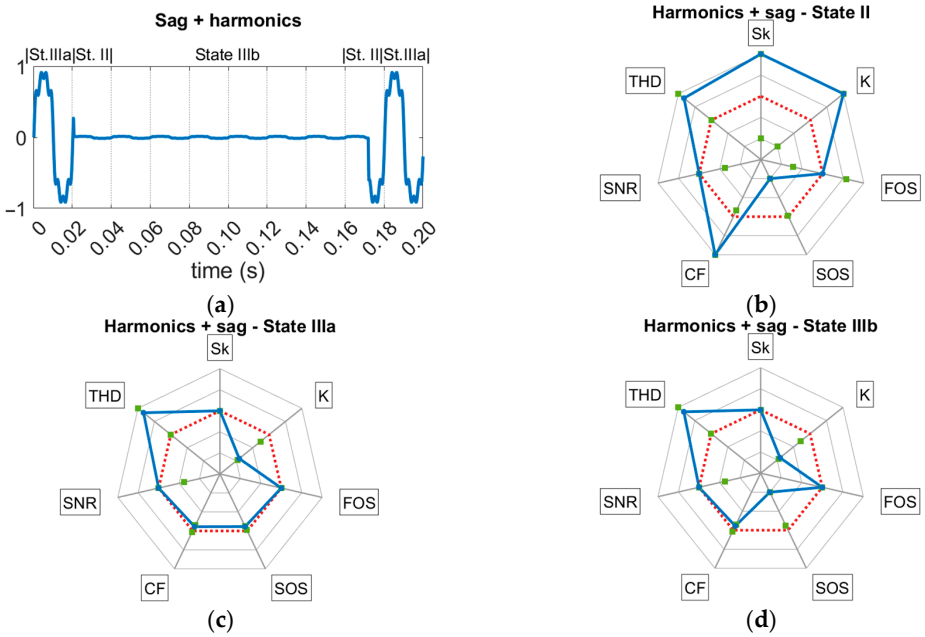

Figure 14. (**a**) Sag + harmonics signal; (**b**) state II behavior pattern for sag + harmonics; (**c**) state III-a behavior pattern for sag + harmonics; (**d**) state III-b behavior pattern for sag + harmonics. Blue line designates the current shape, the red line shows the ideal shape, and the green square marks illustrate maximum and minimum values.

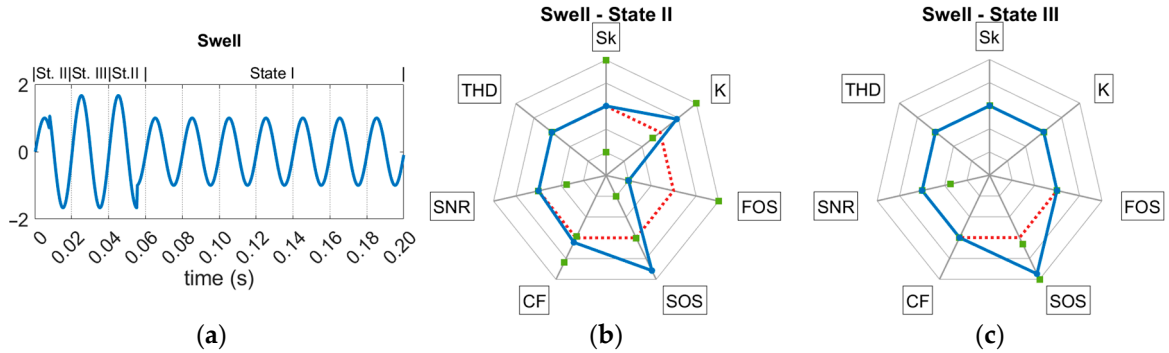

Figure 15. (**a**) Swell signal; (**b**) state II behavior pattern for swells; (**c**) state III behavior pattern for swells. Blue line designates the current shape, the red line shows the ideal shape, and the green square marks illustrate maximum and minimum values.

Table 2. Flicker's maximum and minimum.

Indicator	Max	Min
Sk	0.0145	−0.0143
K	1.6374	1.5203
FOS	0.0302	−0.0291
SOS	0.4329	0.3244
CF	1.6804	1.4256
SNR	80	30
THD	8	8

Table 3. Harmonics' maximum and minimum.

Indicator	Max	Min
Sk	2.2×10^{-15}	-3.7×10^{-15}
K	1.4294	1.2057
FOS	1.5×10^{-15}	-2.2×10^{-15}
SOS	0.2952	0.1987
CF	1.4653	1.2414
SNR	80	30
THD	22	8

Table 4. Impulsive transient's maximum and minimum.

Indicator	Max	Min
Sk	0.0691	−0.0674
K	1.5889	1.4741
FOS	0.0302	−0.0309
SOS	0.3126	0.2282
CF	1.4918	1.4142
SNR	80	30
THD	8	8

Table 5. Notch's maximum and minimum.

Indicator	Max	Min
Sk	0.0761	−0.0314
K	1.5685	1.4903
FOS	0.03494	−0.01491
SOS	0.3145	0.2708
CF	1.4505	1.4114
SNR	80	30
THD	8	8

Table 6. Oscillatory transient's maximum and minimum.

Indicator	Max	Min
Sk	0.2210	−0.3050
K	1.8030	1.4503
FOS	0.1710	−0.1710
SOS	1.8865	0.3095
CF	2.3093	1.3908
SNR	80	30
THD	8	8

Table 7. Spike's maximum and minimum.

Indicator	Max	Min
Sk	0.1122	−0.0523
K	1.6676	1.4404
FOS	0.1329	−0.0274
SOS	0.5521	0.3126
CF	1.9422	1.3874
SNR	80	30
THD	8	8

Table 8. Interruption's maximum and minimum.

Indicator	Max St. II	Min St. II	Max St. III	Min St. III
Sk	0.31	−0.31	2.8×10^{-14}	-1.9×10^{-14}
K	1.80	1.47	1.5	1.5
FOS	0.14	−0.14	4.3×10^{-21}	-8.0×10^{-21}
SOS	0.32	0	0	0
CF	2.51	1.41	1.41	1.41
SNR	80	30	80	30
THD	8	8	8	8

Table 9. Sag's maximum and minimum.

Indicator	Max St. II	Min St. II	Max St. III	Min St. III
Sk	0.31	−0.31	9.8×10^{-16}	-2.4×10^{-15}
K	1.80	1.44	1.5	1.5
FOS	0.12	−0.12	2.4×10^{-16}	-5.7×10^{-16}
SOS	0.31	0	0.17	0
CF	2.51	1.38	1.41	1.41
SNR	80	30	80	30
THD	8	8	8	8

Table 10. Sag + harmonics' maximum and minimum.

Indicator	Max St. II	Min St. II	Max St. III-a	Min St. III-a	Max St. III-b	Min St. III-b
Sk	0.31	−0.31	2.1×10^{-15}	-3.5×10^{-15}	1.6×10^{-15}	-5.7×10^{-15}
K	1.80	1.20	1.42	1.21	1.41	1.21
FOS	0.10	−0.12	1.23	−1.98	5.3×10^{-16}	-1.0×10^{-15}
SOS	0.29	0	0.29	0.20	0.20	0
CF	2.51	1.23	1.45	1.25	1.44	1.25
SNR	80	30	80	30	80	30
THD	22	8	22	8	22	8

Table 11. Swell's maximum and minimum.

Indicator	Max St. II	Min St. II	Max St. III	Min St. III
Sk	0.31	−0.31	1.1×10^{-15}	-2.0×10^{-15}
K	1.80	1.44	1.5	1.5
FOS	0.17	−0.17	7.5×10^{-15}	-1.7×10^{-14}
SOS	10.63	0.31	10.62	0.56
CF	2.07	1.38	1.41	1.41
SNR	80	30	80	30
THD	8	8	8	8

Table 12. Swell + harmonics' maximum and minimum.

Indicator	Max St. II	Min St. II	Max St. III-a	Min St. III-a	Max St. III-b	Min St. III-b
Sk	0.31	−0.31	1.8×10^{-15}	-3.7×10^{-15}	1.7×10^{-15}	-3.6×10^{-15}
K	1.67	1.20	1.41	1.21	1.41	1.21
FOS	0.17	−0.17	1.1×10^{-15}	-2.0×10^{-15}	1.6×10^{-14}	-4.9×10^{-14}
SOS	12.81	0.20	0.29	0.20	14.61	0.30
CF	2.10	1.24	1.45	1.24	1.45	1.24
SNR	80	30	80	30	80	30
THD	22	8	22	8	22	8

As can be seen, some events do not imply the appearance of the three possible states: harmonics, notches and spikes constantly present stability under the event, so these disturbances operate in state III. Flickers and transients do not stabilize; then, state II is shown. Signals with interruptions, sags and swells show all three states.

Furthermore, to analyze complex events, state types must also be considered. For example, for sag + harmonics and swell + harmonics, two types of state III arise: one of them corresponds to stability under the harmonic (state III-a in Figures 15 and 16), and the other type of state III reflects stability under the sag/swell with harmonics (state III-b).

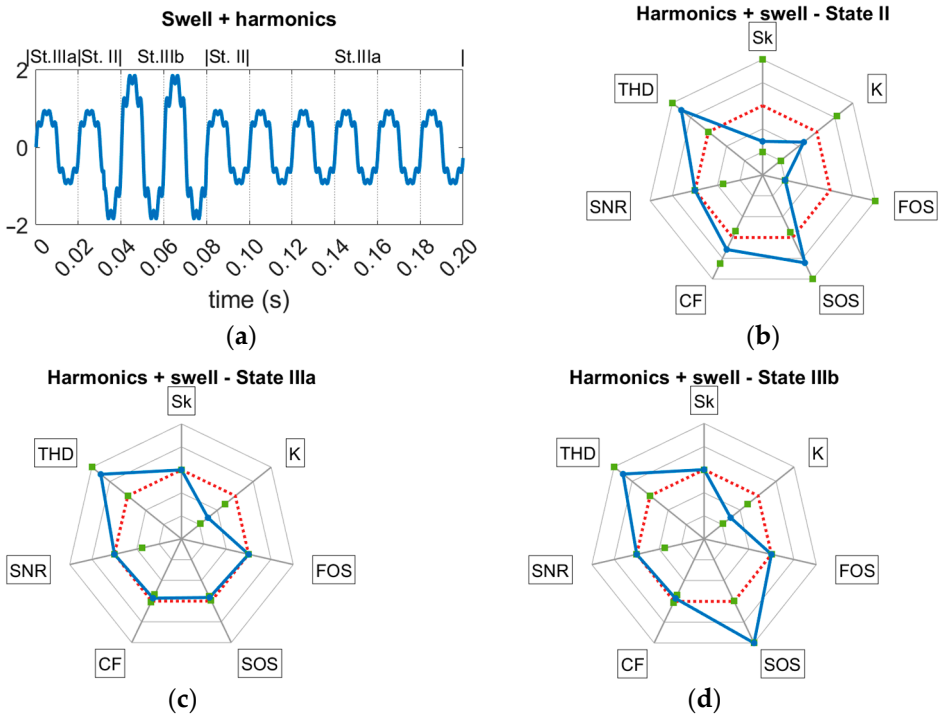

Figure 16. (**a**) Swell + harmonics signal; (**b**) state II behavior pattern for swell + harmonics; (**c**) state III-a behavior pattern for swell + harmonics; (**d**) state III-b behavior pattern for swell + harmonics. Blue line designates the current shape, the red line shows the ideal shape, and the green square marks illustrate maximum and minimum values.

4.2. Radar Charts and Boxplots Comparison

Adhering to the prescribed methodology and once the per-event behavior patterns for synthetic signals are established, hybrid synthetic signals and real signals are processed cycle by cycle and then boxplots are drawn, and the result of the decision tree is obtained for comparative purposes.

To ensure a comprehension of the radar charts analysis produced per cycle, only small segments of the selected signals are presented. The goal is to clearly illustrate the three states discussed in the previous subsection. In all the signals examined from Figures 17–22, the three states have been distinguished. If several cycles under a specific state displayed almost identical radar charts, the authors have simplified the presentation by showing only one of the radar charts, the most representative of which indicates the highest changes in the indices.

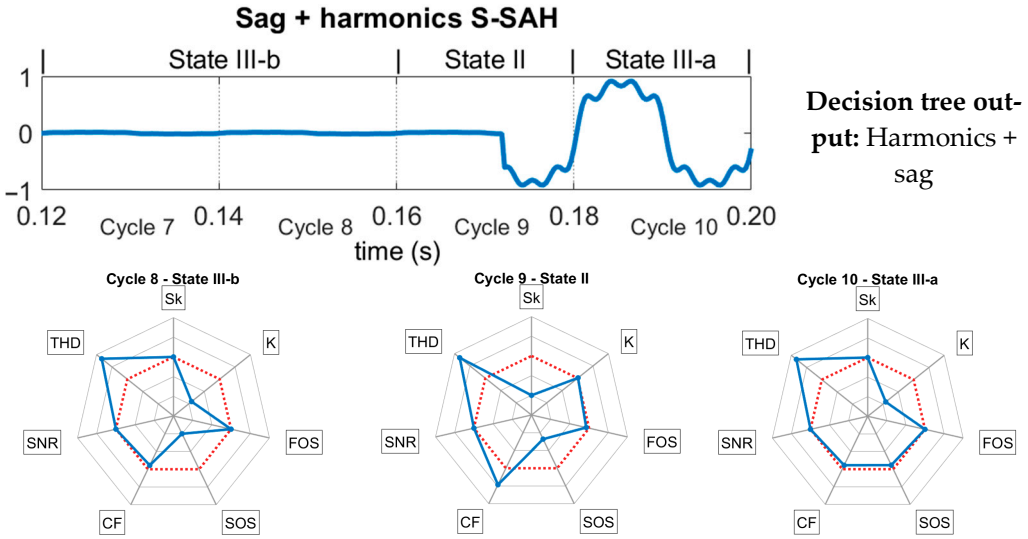

Figure 17. Radar charts of a synthetic 50 Hz signal with harmonics and a sag. Blue line designates the current shape, and the red line shows the ideal shape.

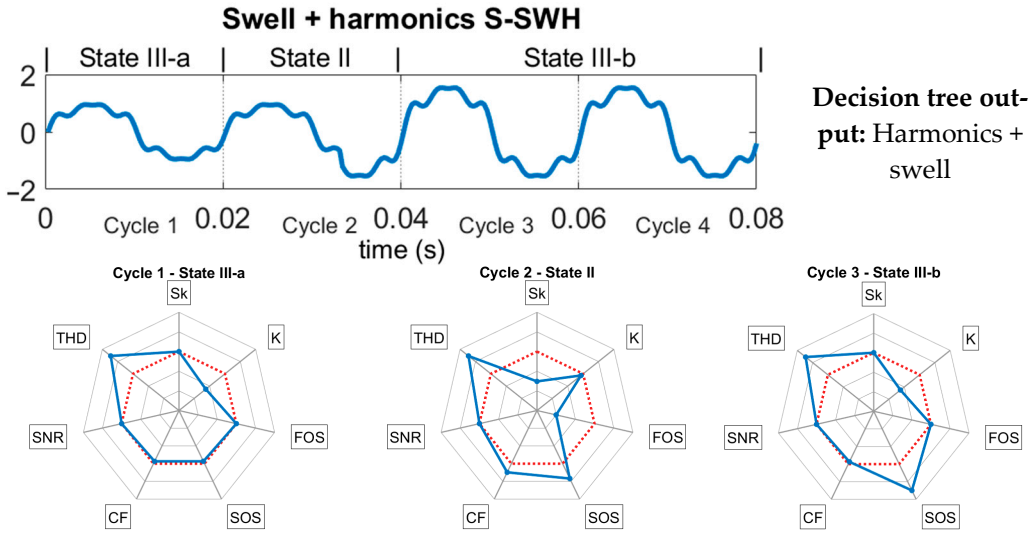

Figure 18. Radar charts of a synthetic 50 Hz signal with harmonics and a swell. Blue line designates the current shape, and the red line shows the ideal shape.

The analysis of this section is as follows:

1. Signal representation on the time domain, where the three states (state I, II and III) and types have been previously identified, illustrating the events analyzed in this subsection: synthetic sag + harmonics and swell + harmonics, and real sag and impulsive transient.
2. A radar chart according to each state is represented, and the output of the decision tree is shown.
3. Boxplot information is analyzed.

4.2.1. Analysis of Synthetic Signals

Since no real hybrid signals are available, the authors have decided to analyze the sag + harmonics S-SAH and swell + harmonics S-SWH signals from the synthetic database, thus providing a projection of the behavior of the visual tool under complex disturbances.

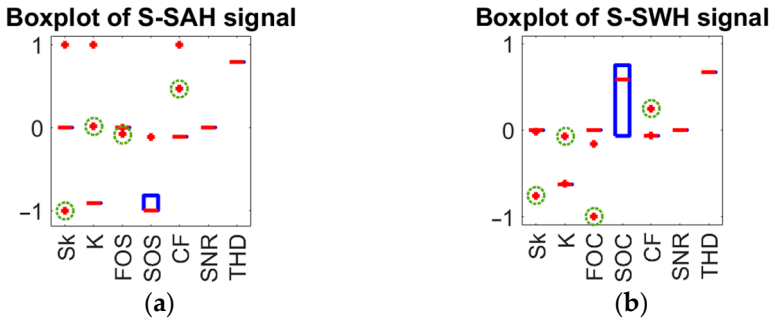

Figure 19. Boxplots of: (**a**) S-SAH signal; (**b**) S-SWH signal. State II values are circled.

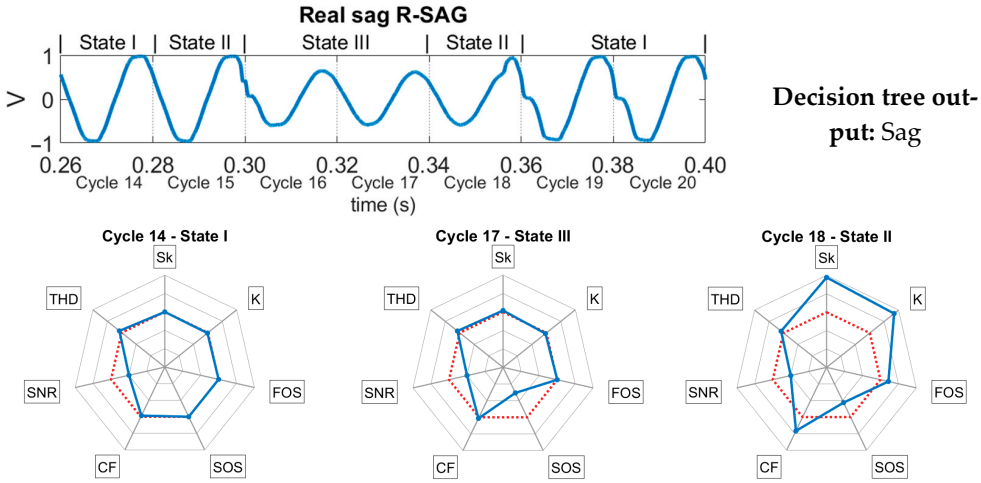

Figure 20. Radar charts of a real 50 Hz signal with a sag. Blue line designates the current shape, and the red line shows the ideal shape.

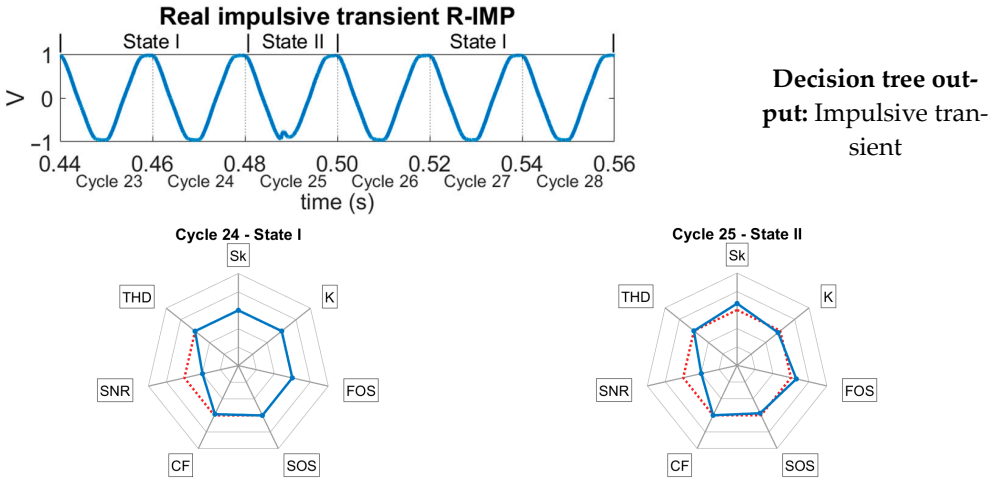

Figure 21. Radar charts of a real 50 Hz signal with an impulsive transient. Blue line designates the current shape, and the red line shows the ideal shape.

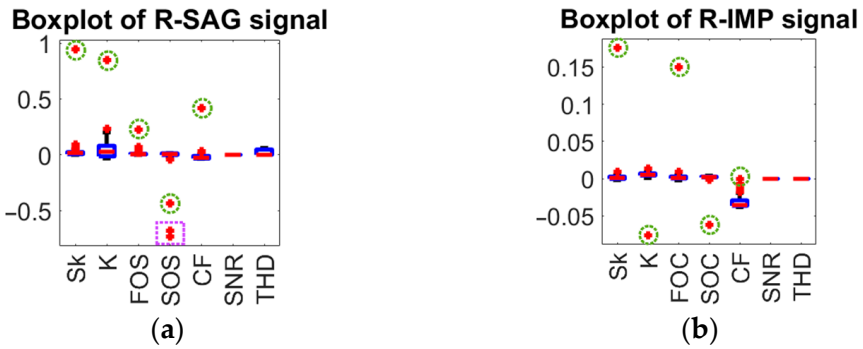

Figure 22. Boxplots of (**a**) R-SAG signal; (**b**) R-IMP signal. State II values are circled. State III SOS values are also highlighted.

The radar charts of S-SAH (Figure 17) and S-SWH (Figure 18) signals correspond to the patterns established for both events, and the decision tree correctly classifies the types of events. THD reflects the presence of harmonics. Furthermore, Sk and FOS are immune to harmonics in states III-a and III-b, and their value is altered in state II, while the kurtosis value is quite affected by harmonics (states III-a and III-b). K and CF also vary under this unstable state. The values acquired by these indicators (Sk, K, FOS and CF) in state II are the so-called "transitional values". The SOS value varies proportionally to the amplitude of the waveform: in the states with sag (II and III-b in Figure 16), SOS decreases, and under a swell, the value obtained increases (Figure 17). If the SOS value reaches a value lower than 3.12×10^{-7}, then the event is an interruption. This value is named a "differentiating value."

Boxplots in Figure 19 correspond to S-SAH (Figure 19a) and S-SWH (Figure 19b) signals. The outliers from states II shown in Figures 17 and 18 have been circled. Notice that for the complete signal (10 cycles), in both cases, two cycles in state II are located through the outliers. Based on the boxplots, the most appropriate indicators to analyze each type of PQ event are defined. The distance from the median and box to zero in the diagrams in Figure 19 of THD, SOS and K indicates these indicators to be more suitable for detecting harmonics with sag/swell.

To determine from the boxplots when a signal presents a PQ event, Table 13 establishes tolerance bands for normal signal fluctuations. Indicator values outside these bands are considered statistically significant deviations likely caused by an event.

Table 13. Tolerance bands for normal signal behavior in boxplots.

Indicator	Lower Limit	Upper Limit
Skewness	−0.0244	0.0266
Kurtosis	1.4771	1.5306
Fifth-order statistic	−0.0144	0.0161
Sixth-order statistic	0.2854	0.3403
Crest factor	1.4027	1.5193
SNR	80	160
THD	0	8

4.2.2. Analysis of Real Signals

The evolution in time of a real sag and an impulsive transient is shown through their radar charts per cycle in Figures 20 and 21. Since the SNR value is 40 dB, the presence of Gaussian noise causes a slight variation in the indicators with respect to the nominal values in state I. Despite this fact, states II and III are notable and distinguishable between them.

Figure 22 shows the boxplots of the indicators' values obtained from R-SAG (Figure 22a) and R-IMP (Figure 22b) signals. The outliers of state II of Figures 20 and 21 have been circled. Unlike boxplots drawn from synthetic signals, for real signals, a box is obtained around the nominal values, and even outliers appear close to these values due to noise. The short sag duration in R-SAG signal versus the total signal duration causes the values acquired by SOS during the event to be marked as outliers (boxed in purple in Figure 22a).

4.3. Tool Accuracy

The location of synthetic events from the Synthetic Power Quality Disturbances database using the radar chart tool with the decision tree algorithm has yielded 83.33% to 100% satisfactory results, which are higher than the detection percentages of boxplots, as shown in Table 14.

Table 14. Percentage of event satisfactorily detected by the proposed tool.

Database	PQ Event	System Radar + Decision Tree Detection (%)	Boxplot Detection (%)
Synthetic Power Quality Disturbances	Flicker	100	99
	Harmonics	100	100
	Impulsive transient	99	46
	Interruption	91	90
	Notch	90	27
	Oscillatory transient	90	58
	Sag	97	92
	Spike	98	68
	Swell	91	90
	Sag + harmonics	98	97
	Swell + harmonics	100	100
Real-life Power Quality Events	Sag	96.15	76.92
	Impulsive transient	83.33	23.81

The detection percentages for the radar chart + decision tree system were obtained based on the quantity of event correctly classified by the decision tree. An event is considered satisfactorily detected by the boxplot when the limits established in Table 13 are exceeded.

As a first observation when treating real sag signals, it can be said that the alteration with respect to the ideal pattern of the radar allows us to conclude in 96.15% of the cases that a sag electrical event in the presence of distortion has occurred. For real impulsive transient signals, the detection percentage is 83.33% compared to 99% for synthetic impulsive events. In both cases, there is a strong correlation between an altered radar pattern and the existence of a disturbance in the time domain. The detection capability of the radar + decision tree system significantly surpasses that of boxplots by up to 50% for notches, oscillatory transients, spikes, and synthetic and real impulsive transients.

The error percentages of the radar + decision tree system may be due to Gaussian noise affecting the indicators beyond the alteration caused by the event itself or to the observation window not being completely reliable. In that case, the error could be reduced by analyzing the same signal multiple times while varying the starting point of the cycles; however, this approach would risk saturating the system memory.

5. Discussion

In this section, the authors delve into the benefits and limitations of the visual tool developed for power quality analysis, considering both synthetic and real signals.

Although clear patterns have been established in synthetic signals corresponding to at least 90% of the events, the presence of noise and distortion of real signals causes the correspondence between the expected behavior patterns and reality to be at least 83.33% for real impulsive transient events, and 96.15% for real sags, confirming a margin of error for the tool. However, the event detection through the proposed system surpasses traditional tools, such as boxplots, in all cases. Furthermore, unlike purely visual methods, the decision tree provides a quantitative system for classifying events.

Despite alterations due to noise and distortion in real signals, the pattern corresponding to each state remains distinguishable. Although the tool does not provide data on the exact moment an event occurs or begins, it does allow for locating the signal cycle in which the event takes place, as long as the signal lasts a minimum of 10 cycles, therefore providing a range of 0.02 s within which the event clearly appears. However, when it comes to continuous real-time visualization, such frequency (one cycle at 50 Hz) is unnecessary and cognitively inefficient. A more practical implementation would involve processing overlapping windows of 100 cycles (2 s) and displaying only the most altered cycle within that interval. This would ensure meaningful human interpretability while retaining a near-real-time response capability.

From a computational standpoint, prior evaluations of the algorithm have shown execution times of up to 0.36 s per 1000 data points under favorable conditions, suggesting that near-real-time operation could be achievable with an optimized implementation (e.g., using compiled languages or parallel processing). Moreover, since the analysis is inherently cycle by cycle, the method is structurally well suited to real-time monitoring systems, where visualization or alert generation can be decoupled from raw computation and scheduled at lower, perceptually meaningful frequencies.

An improvement to further optimize the simplicity of the measurement system could involve the incorporation of a color-coded system. This system would assign colors to the radar chart area based on the optimal behavior of the signal. For example, if an event is detected, the area enclosed in the heptagon could be highlighted in red for quick identification.

6. Conclusions

A comprehensive examination of both traditional and non-traditional indicators of power quality has been undertaken, drawing from relevant references to develop a convenient power quality visualization tool. This tool has been 96.15% suitable for capturing and analyzing sag events with distortion in electrical signals and 83.33% for impulsive transient signals, showing significant potential for application in real-world power grid environments marked by non-linear loads and non-Gaussian behaviors. Notably, it outperforms traditional tools, such as boxplots, in detecting impulsive transients, notches, oscillatory transients, and spikes.

The study of these indicators plays a key role in this article, offering valuable insights that expand our knowledge in the field of power quality, establishing nominal values for fifth- and sixth-order statistics, shedding light on scenarios where HOS are crucial, and providing behavior patterns of indicators under multiple events. The sixth-order statistic is found to be the most appropriate indicator for detecting RMS variation events, such as interruptions, sags and swells (Figures 17, 18 and 20). Variations of kurtosis and THD, as opposed to Sk and FOS not affected by harmonics, also facilitate the detection of simple and complex harmonic events (Figures 17 and 18).

Finally, through the behavioral patterns of the radar chart with the decision tree, PQ events are visually distinguished from each other and classified—an arduous task when using more traditional visualization tools, such as boxplots. Although boxplots allow

for checking the presence of events in a signal based on the total variation ranges of the indicators, they make it difficult to differentiate most events by simple observation.

Author Contributions: Conceptualization, P.R.-C., O.F.-O. and J.-J.G.-d.-l.-R.; methodology, P.R.-C., O.F.-O. and J.-J.G.-d.-l.-R.; validation, P.R.-C., O.F.-O. and J.-J.G.-d.-l.-R.; formal analysis, P.R.-C.; investigation, P.R.-C.; resources, P.R.-C.; data curation, P.R.-C. and O.F.-O.; writing—original draft preparation, P.R.-C.; writing—review and editing, P.R.-C., O.F.-O. and J.-J.G.-d.-l.-R.; visualization, P.R.-C., O.F.-O. and J.-J.G.-d.-l.-R.; supervision, O.F.-O. and J.-J.G.-d.-l.-R.; project administration, P.R.-C. All authors have read and agreed to the published version of the manuscript.

Funding: This research received no external funding.

Institutional Review Board Statement: Not applicable.

Informed Consent Statement: Not applicable.

Data Availability Statement: Data available on request from the authors.

Acknowledgments: The authors express their gratitude to the Spanish Ministry of Science and Education and the State Investigation Agency for funding the research project PID2019-108953RB-C21, entitled 'Strategies for Aggregated Generation of Photo-Voltaic Plants-Energy and Meteorological Data' (SAGPV-EMOD), and the Andalusian Government for supporting the Research Group PAIDI-TIC-168, in Computational Instrumentation and Industrial Electronics (ICEI).

Conflicts of Interest: The authors declare no conflicts of interest.

Abbreviations

The following abbreviations are used in this manuscript:

AI	artificial intelligence
CF	crest factor
EDA	exploratory data analysis
EDM	energy data management
FOS	fifth-order statistic
HOS	higher-order statistic
K	kurtosis
PQ	power quality
Sk	skewness
SNR	signal to noise ratio
SOS	sixth-order statistic
THD	total harmonic distortion

References

1. Martinez, R.; Castro, P.; Arroyo, A.; Manana, M.; Galan, N.; Moreno, F.S.; Bustamante, S.; Laso, A. Techniques to Locate the Origin of Power Quality Disturbances in a Power System: A Review. *Sustainability* **2022**, *14*, 7428. [CrossRef]
2. *EN 50160*; Voltage Characteristics of Electricity Supplied by Public Electricity Networks. AENOR: Madrid, Spain, 2023.
3. Chang, S.; Deng, Y.; Zhang, Y.; Zhao, Q.; Wang, R.; Zhang, K. An Advanced Scheme for Range Ambiguity Suppression of Spaceborne SAR Based on Blind Source Separation. *IEEE Trans. Geosci. Remote Sens.* **2022**, *60*, 5230112. [CrossRef]
4. Chawda, G.S.; Shaik, A.G.; Shaik, M.; Padmanaban, S.; Holm-Nielsen, J.B.; Mahela, O.P.; Kaliannan, P. Comprehensive Review on Detection and Classification of Power Quality Disturbances in Utility Grid With Renewable Energy Penetration. *IEEE Access* **2020**, *8*, 146807–146830. [CrossRef]
5. Khaleel, M.; Abulifa, S.A.; Abulifa, A.A. Artificial Intelligent Techniques for Identifying the Cause of Disturbances in the Power Grid. *Brill. Res. Artif. Intell.* **2023**, *3*, 19–31. [CrossRef]
6. de Oliveira, R.A.; Bollen, M.H.J. Deep learning for power quality. *Electr. Power Syst. Res.* **2023**, *214*, 108887.
7. Yan, Y.; Chen, K.; Geng, H.; Fan, W.; Zhou, X. A Review on Intelligent Detection and Classification of Power Quality Disturbances: Trends, Methodologies, and Prospects. *Comput. Model. Eng. Sci.* **2023**, *137*, 1345–1379. [CrossRef]
8. Caicedo, J.E.; Agudelo-Martínez, D.; Rivas-Trujillo, E.; Meyer, J. A systematic review of real-time detection and classification of power quality disturbances. *Prot. Control. Mod. Power Syst.* **2023**, *8*, 3. [CrossRef]

9. Palomares-Salas, J.C.; González de la Rosa, J.J.; Agüera-Pérez, A.; Moreno-Muñoz, A. Intelligent Methods for Characterization of Electrical Power Quality Signals using Higher Order Statistical Features. *Przegląd Elektrotechniczny* **2012**, *8*, 236.
10. Saini, M.K.; Beniwal, R.K. Detection and classification of power quality disturbances in wind-grid integrated system using fast time-time transform and small residual-extreme learning machine. *Int. Trans. Electr. Energy Syst.* **2018**, *28*, e2519. [CrossRef]
11. Romero-Ramirez, L.A.; Elvira-Ortiz, D.A.; Jaen-Cuellar, A.Y.; Morinigo-Sotelo, D.; Osornio-Rios, R.A.; Romero-Troncoso, R.D.J. Methodology based on higher-order statistics and genetic algorithms for the classification of power quality disturbances. *IET Gener. Transm. Distrib.* **2020**, *14*, 4580–4592. [CrossRef]
12. Florencias-Oliveros, O.; González-de-la-Rosa, J.-J.; Agüera-Pérez, A.; Palomares-Salas, J.-C. Power quality event dynamics characterization via 2D trajectories using deviations of higher-order statistics. *Measurement* **2018**, *125*, 350–359. [CrossRef]
13. Zanoni, M.; Chiappa, C.; Chiumeo, R.; Tenti, L.; Shadmehr, H. Higher-Order Statistics for Voltage Dips Characterization on Italian MV Networks. In Proceedings of the 2020 AEIT International Annual Conference (AEIT), Catania, Italy, 23–25 September 2020; pp. 1–6.
14. Beniwal, R.K.; Saini, M.K.; Nayyar, A.; Qureshi, B.; Aggarwal, A. A Critical Analysis of Methodologies for Detection and Classification of Power Quality Events in Smart Grid. *IEEE Access* **2021**, *9*, 83507–83534. [CrossRef]
15. Shin, Y.-J.; Powers, E.J.; Grady, M.; Arapostathis, A. Power Quality Indices for Transient Disturbances. *IEEE Trans. Power Deliv.* **2006**, *21*, 253–261. [CrossRef]
16. Axelberg, P.G.V.; Gu, I.Y.H.; Bollen, M.H.J. Support vector machine for classification of voltage disturbances. *IEEE Trans. Power Deliv.* **2007**, *22*, 1297–1303. [CrossRef]
17. Ribeiro, E.G.; Dias, G.L.; Barbosa, B.H.G.; Ferreira, D.D. Real-time system for automatic classification of power quality disturbances. In Proceedings of the International Conference on Harmonics and Quality of Power, ICHQP, Belo Horizonte, Brazil, 16–19 October 2016; pp. 908–913.
18. Jamali, S.; Farsa, A.R.; Ghaffarzadeh, N. Identification of optimal features for fast and accurate classification of power quality disturbances. *Measurement* **2018**, *116*, 565–574. [CrossRef]
19. Shen, Y.; Abubakar, M.; Liu, H.; Hussain, F. Power Quality Disturbance Monitoring and Classification Based on Improved PCA and Convolution Neural Network for Wind-Grid Distribution Systems. *Energies* **2019**, *12*, 1280. [CrossRef]
20. Thirumala, K.; Pal, S.; Jain, T.; Umarikar, A.C. A classification method for multiple power quality disturbances using EWT based adaptive filtering and multiclass SVM. *Neurocomputing* **2019**, *334*, 265–274. [CrossRef]
21. Florencias-Oliveros, O.; Gonzalez-de-la-Rosa, J.-J.; Sierra-Fernandez, J.-M.; Aguera-Perez, A.; Espinosa-Gavira, M.-J.; Palomares-Salas, J.-C. Site Characterization Index for Continuous Power Quality Monitoring Based on Higher-order Statistics. *J. Mod. Power Syst. Clean Energy* **2022**, *10*, 222–231. [CrossRef]
22. Ventura, J.; Martinez, F.; Castro-Santos, L.; Filgueira-Vizoso, A.; Alcayde, A.; Montoya, F.G. Characterisation of Electrical Power Systems Based on Electrical Curves and their properties. *Renew. Energy Power Qual. J.* **2023**, *21*, 589–593. [CrossRef]
23. Ignatova, V.; Villard, D.; Hypolite, J.M. Simple indicators for an effective Power Quality monitoring and analysis. In Proceedings of the 2015 IEEE 15th International Conference on Environment and Electrical Engineering, EEEIC 2015-Conference Proceedings, Rome, Italy, 10–13 June 2015; pp. 1104–1108.
24. Kattmann, C.; Tenbohlen, S. Visualization of power quality data. In Proceedings of the 2017 IEEE Manchester PowerTech, Manchester, UK, 18–22 June 2017.
25. Machlev, R.; Chachkes, A.; Belikov, J.; Beck, Y.; Levron, Y. Open source dataset generator for power quality disturbances with deep-learning reference classifiers. *Electr. Power Syst. Res.* **2021**, *195*, 107152. [CrossRef]
26. Florencias-Oliveros, O.; Espinosa-Gavira, M.J.; González de la Rosa, J.-J.; Agüera-Pérez, A.; Palomares-Salas, J.C.; Sierra-Fernández, J.M. *Real-Life Power Quality Sags*; IEEE Dataport; Institute of Electrical and Electronics Engineers (IEEE): Piscataway, NJ, USA, 2017.
27. Florencias-Oliveros, O.; Espinosa-Gavira, M.J.; González-de-la-Rosa, J.J.; Agüera-Pérez, A.; Palomares-Salas, J.C.; Sierra-Fernández, J.M. *Real-Life Power Quality Transients*; Institute of Electrical and Electronics Engineers (IEEE): Piscataway, NJ, USA, 2017.
28. Mahela, O.P.; Shaik, A.G.; Khan, B.; Mahla, R.; Alhelou, H.H. Recognition of Complex Power Quality Disturbances Using S-Transform Based Ruled Decision Tree. *IEEE Access* **2020**, *8*, 173530–173547. [CrossRef]
29. Masoum, M.A.S.; Jamali, S.; Ghaffarzadeh, N. Detection and classification of power quality disturbances using discrete wavelet transform and wavelet networks. *IET Sci. Meas. Technol.* **2010**, *4*, 193–205. [CrossRef]
30. Tomic, J.J.; Kusljevic, M.D.; Vujicic, V.V. A New Power System Digital Harmonic Analyzer. *IEEE Trans. Power Deliv.* **2007**, *22*, 772–780. [CrossRef]

31. Santos, R.Y.C.; Moreno, E.D.; Estombelo-Montesco, C.A. SED-Bench: Benchmark for Simulated Electrical Disturbance. *IEEE Trans. Instrum. Meas.* **2020**, *69*, 3954–3961. [CrossRef]
32. *IEC 61000-4-7*; Electromagnetic Compatibility (EMC). Testing and Measurement Techniques-General Guide on Harmonics and Interharmonics Measurements and Instrumentation, for Power Supply Systems and Equipment Connected Thereto. International Electrotechnical Commission (IEC): Geneva, Switzerland, 2002.